JPE 16-4-11

http://dx.doi.org/10.6113/JPE.2016.16.4.1346
ISSN(Print): 1598-2092 / ISSN(Online): 2093-4718

Gain Design of an Adaptive Full-order Observer Using a Pole Placement Technique for Speed Sensorless Induction Motor Drives

Anno Yoo*, Sang-Heon Han**, Young Ik Son**, Young-Doo Yoon†, and Chanook Hong***

*General Motors, Pontiac, MI, United States
**,†Dept. of Electrical Eng., Myongji University, Yongin, Korea
***LSIS Co., Ltd., Anyang, Korea

Abstract

This paper proposes a design guideline for the feedback gain of the adaptive full-order observer in the speed sensorless control of induction machines. The performance of the adaptive full-order observer is dependent on its feedback gain. This paper presents a pole placement method for the observer feedback gain design to improve the estimation performance of the speed adaptive observer. In the proposed method, the observer poles can be chosen independently of the induction motor poles. Instead, they can be positioned according to the operating speed. An analysis and experimental results obtained with the proposed method reveals better performances under general operating conditions.

Key words: Adaptive speed observer, Full-order observer, Induction motor, Pole placement, Sensorless control

I. INTRODUCTION

Induction motors have many attractive characteristics, such as a robust design, relatively low cost, reasonable size, efficiency, and low maintenance. Thus, they are widely used for conventional drive applications and high-performance applications [1], [2]. Most of these applications require adjustable-speed drives and/or suitable control performances, such as a wide operating range and appropriate dynamics. Vector control (field-oriented control, FOC) theory has become a standard technology in the high-performance induction motor drives in speed/torque control areas. However, the FOC strategy requires information on the rotor position [3]. Therefore, a rotor position sensor (e.g., a resolver and an encoder) is installed at the rotor shaft. However, these sensors increase the cost and volume of drive systems, and reduce their reliability.

Speed sensorless control has become an indispensable function of general-purpose inverters, due to the practical benefits related to rotor position sensors, which include reductions in mechanical volume and cost. Over the past several decades, significant efforts have been devoted to the development of speed sensorless drives for induction machines. Since the application areas of speed sensorless controls have broadened, many inverter manufacturers have concentrated on improving the performance of speed sensorless controls and have developed their own algorithms. There have been numerous studies on the speed sensorless control of induction machine drives [4]-[19]. Mixed structures based on the voltage model and rotor flux model have been proposed [4], [5]. However, although these methods demonstrated acceptable performance above the medium speeds in which the voltage model was dominant, the performance was degraded at low speeds due to inaccuracies in the rotor flux model.

In [6], an adaptive full-order observer, which is responsible for estimating the rotor speed and rotor flux from the stator current and voltage, has been presented. It has been widely used in industrial fields for speed sensorless control due to its performance, particularly under low-speed operation.

Several years ago, Sanwongwanich et al. [7]-[9] presented general stability conditions for speed sensorless control, based on the adaptive full-order observer. They demonstrated that the

Manuscript received Jan. 2, 2016; accepted Mar. 21, 2016
Recommended for publication by Associate Editor Kwang-Woon Lee.
†Corresponding Author: ydyoon@mju.ac.kr
Tel: +82-31-330-6833, Myongji University
*General Motors, United States
**Dept. of Electrical Eng., Myongji University, Korea
***LSIS Co., Ltd., Korea

adaptive full-order observer has unstable operating regions in regenerating operations, and that these unstable regions were determined by the selection of the feedback gain. Similar conditions were presented for the reduced-order observer [10]. With a proper gain design, the observers can estimate the rotor flux for most of the operating points, with the exception of those for the zero synchronous frequency.

In practical applications, the stator resistance of induction machines varies due to temperature changes in the machines, which may cause unstable operation, especially at low speeds [11]. To improve stability, several adaptation methods have been proposed for stator resistance [12]-[17]. Studies on numerical stability analysis [14] and analytical stability conditions [16] have been described. These adaption methods can be implemented along with rotor flux and speed estimation algorithms [16], [17], with the stability of the speed sensorless control being somewhat guaranteed even under variations of the stator resistance.

Along with these stability analyses, several gain selection strategies for adaptive full-order observers have been developed to achieve stability [7], [9], [16]-[20]. These studies showed that the unstable region can be avoided with the feedback gain. They also showed that reasonable control performances at low speed can be achieved. However, at medium speeds, the flux estimation performance is degraded [7], [20], because the estimation bandwidths of the observers may be insufficient when compared with the operation frequency. In addition, the observers may possess under-damping characteristics.

This paper presents an analysis of the feedback gains of adaptive full-order observers to cope with the instability phenomenon and to improve the performance of speed sensorless control. A pole placement method is used to design a gain matrix. The observer poles can be placed in arbitrary positions; i.e., the observer poles can be chosen independently of the induction motor poles. Based on this insight, the observer gain is designed to ensure stability conditions, and to provide accurate estimates of the flux and speed over a range of operating points.

II. ADAPTIVE FULL-ORDER OBSERVER

Stator current and rotor flux of induction machines in the stationary reference frame are given in (1) and (2), as follows:

$$\frac{d}{dt}\mathbf{i}_s^s = -\left\{\frac{R_s}{\sigma L_s}+\frac{(1-\sigma)}{\sigma\tau_r}\right\}\mathbf{i}_s^s + \frac{L_m}{\sigma L_s L_r}\frac{1}{\tau_r}\boldsymbol{\lambda}_r^s - \frac{L_m}{\sigma L_s L_r} j\omega_r \boldsymbol{\lambda}_r^s + \frac{1}{\sigma L_s}\mathbf{V}_s^s \quad (1)$$

$$\frac{d}{dt}\boldsymbol{\lambda}_r^s = \frac{L_m}{\tau_r}\mathbf{i}_s^s - \frac{1}{\tau_r}\boldsymbol{\lambda}_r^s + j\omega_r\boldsymbol{\lambda}_r^s \quad (2)$$

where $\mathbf{V}_s^s$, $\mathbf{i}_s^s$, $\boldsymbol{\lambda}_r^s$, R_s, L_s, L_m, L_r, τ_r, σ and ω_r represent the stator voltage, stator current, rotor flux, stator resistance, stator inductance, mutual inductance, rotor inductance, rotor time constant, leakage factor $\left(\sigma = 1 - L_m^2/L_s L_r\right)$, and electrical rotor speed, respectively. By selecting the stator current and the rotor flux as state variables, the induction machine can be modeled as follows:

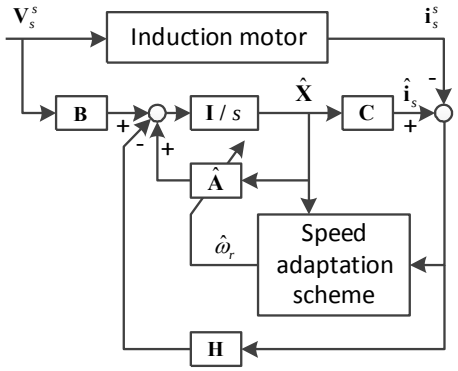

Fig. 1. Block diagram of the speed adaptive full-order observer.

$$\frac{d}{dt}\begin{bmatrix}\mathbf{i}_s\\ \boldsymbol{\lambda}_r\end{bmatrix} = \begin{bmatrix}\mathbf{A}_{11} & \mathbf{A}_{12}\\ \mathbf{A}_{21} & \mathbf{A}_{22}\end{bmatrix}\begin{bmatrix}\mathbf{i}_s\\ \boldsymbol{\lambda}_r\end{bmatrix} + \begin{bmatrix}\mathbf{B}_1\\ 0\end{bmatrix}\mathbf{V}_s = \mathbf{AX} + \mathbf{BV}_s \quad (3)$$

$$\mathbf{i_s} = \mathbf{CX} \quad (4)$$

where $\mathbf{X} = \left[i_{ds}^s\ i_{qs}^s\ \lambda_{dr}^s\ \lambda_{qr}^s\right]^T$, $\mathbf{i}_s = \left[i_{ds}^s\ i_{qs}^s\right]^T$, $\boldsymbol{\lambda}_r = \left[\lambda_{dr}^s\ \lambda_{qr}^s\right]^T$,

$$\mathbf{A}_{11} = -\left\{\frac{R_s}{\sigma L_s}+\frac{(1-\sigma)}{\sigma\tau_r}\right\}\mathbf{I} = a_{r11}\mathbf{I},$$

$$\mathbf{A}_{12} = \frac{L_m}{\sigma L_s L_r}\left\{\left(\frac{1}{\tau_r}\right)\mathbf{I} - \omega_r\mathbf{J}\right\} = a_{r12}\mathbf{I} + a_{i12}\mathbf{J},$$

$$\mathbf{A}_{21} = \frac{L_m}{\tau_r}\mathbf{I} = a_{r21}\mathbf{I},\quad \mathbf{A}_{22} = -\left(\frac{1}{\tau_r}\right)\mathbf{I} + \omega_r\mathbf{J} = a_{r22}\mathbf{I} + a_{i22}\mathbf{J},$$

$$\mathbf{B}_1 = \frac{1}{\sigma L_s}\mathbf{I} = b_1\mathbf{I},\quad \mathbf{C} = \begin{bmatrix}\mathbf{I} & 0\end{bmatrix},\quad \mathbf{I} = \begin{bmatrix}1 & 0\\ 0 & 1\end{bmatrix},\quad \mathbf{J} = \begin{bmatrix}0 & -1\\ 1 & 0\end{bmatrix}.$$

With the given state variables, a adaptive full-order observer [6] can be designed as follows, based on the block diagram shown in Fig. 1.

$$\frac{d}{dt}\begin{bmatrix}\hat{\mathbf{i}}_s\\ \hat{\boldsymbol{\lambda}}_r\end{bmatrix} = \begin{bmatrix}\mathbf{A}_{11} & \hat{\mathbf{A}}_{12}\\ \mathbf{A}_{21} & \hat{\mathbf{A}}_{22}\end{bmatrix}\begin{bmatrix}\hat{\mathbf{i}}_s\\ \hat{\boldsymbol{\lambda}}_r\end{bmatrix} + \begin{bmatrix}\mathbf{B}_1\\ 0\end{bmatrix}\mathbf{V}_s - \begin{bmatrix}\mathbf{H}_1\\ \mathbf{H}_2\end{bmatrix}\left(\hat{\mathbf{i}}_s - \mathbf{i}_s\right) \quad (5)$$

where $\hat{\mathbf{A}}_{12} = \frac{L_m}{\sigma L_s L_r}\left\{\left(\frac{1}{\tau_r}\right)\mathbf{I} - \hat{\omega}_r\mathbf{J}\right\}$ and $\hat{\mathbf{A}}_{22} = -\left(\frac{1}{\tau_r}\right)\mathbf{I} + \hat{\omega}_r\mathbf{J}$, and $\mathbf{H}_1$ and $\mathbf{H}_2$ correspond to the arbitrary gain matrix of the adaptive full-order observer. Using (3) and (5), the error matrix is given by:

$$\frac{d}{dt}\begin{bmatrix}\mathbf{e_i}\\ \mathbf{e}_\lambda\end{bmatrix} = \begin{bmatrix}\mathbf{A}_{11}-\mathbf{H}_1 & \mathbf{A}_{12}\\ \mathbf{A}_{21}-\mathbf{H}_2 & \mathbf{A}_{22}\end{bmatrix}\begin{bmatrix}\mathbf{e_i}\\ \mathbf{e}_\lambda\end{bmatrix} + \begin{bmatrix}0 & -\Delta\omega_r/c\cdot\mathbf{J}\\ 0 & \Delta\omega_r\cdot\mathbf{J}\end{bmatrix}\begin{bmatrix}\hat{\mathbf{i}}_s\\ \hat{\boldsymbol{\lambda}}_r\end{bmatrix} \quad (6)$$

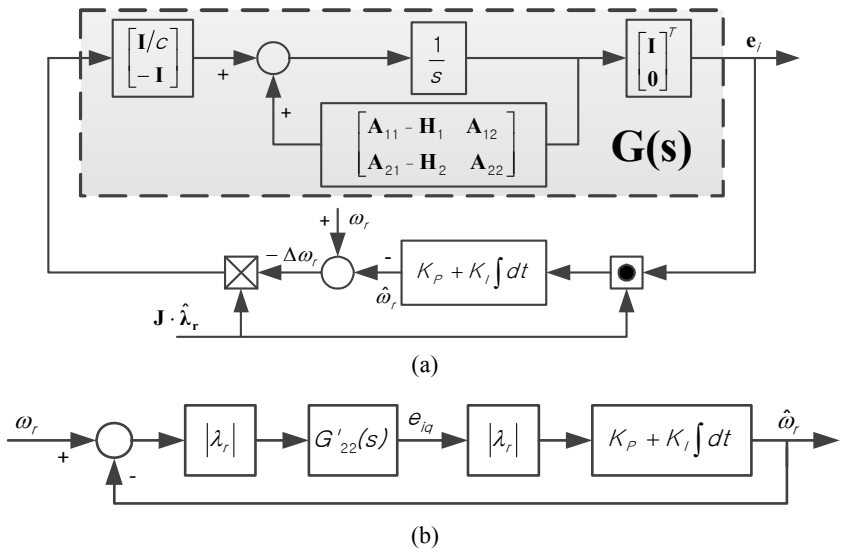

Fig. 2. Block diagram of speed estimation. (a) in the stationary reference frame, and (b) in the rotor flux reference frame.

where $\mathbf{e_i} = \hat{\mathbf{i}}_s - \mathbf{i}_s$, $\mathbf{e}_\lambda = \hat{\boldsymbol{\lambda}}_r - \boldsymbol{\lambda}_r$, $\Delta\omega_r = \hat{\omega}_r - \omega_r$ and $c = \dfrac{\sigma L_s L_r}{L_m}$.

Since the designed adaptive full-order observer estimates the rotor speed from the difference between the real stator current and the estimated stator current, the relationship between the estimation error of the stator current, $\mathbf{e_i}$ and the rotor speed estimation error, $\Delta\omega_r$ can be rewritten as (7) [7]:

$$\begin{aligned}\mathbf{e_i} &= \frac{s}{c}\left[s^2\mathbf{I} + s(\mathbf{H}_1 - \mathbf{A}_{11} - \mathbf{A}_{22}) - \mathbf{A}_{22}\left(\mathbf{H}_1 - \mathbf{A}_{11} + \frac{\mathbf{H}_2 - \mathbf{A}_{21}}{c}\right)\right]^{-1} \\ &\quad \times(\omega_r - \hat{\omega}_r)\mathbf{J}\hat{\boldsymbol{\lambda}}_r \\ &= \mathbf{G}(s)\left[\mathbf{J}\hat{\boldsymbol{\lambda}}_r(\omega_r - \hat{\omega}_r)\right]\end{aligned} \tag{7}$$

where $\mathbf{G}(s) = \dfrac{s}{c}\left[s^2\mathbf{I} + (x\mathbf{I} + y\mathbf{J})s + m\mathbf{I} + n\mathbf{J}\right]^{-1}$, $\mathbf{H}_1 = h_1\mathbf{I} + h_2\mathbf{J}$,

$\mathbf{H}_2 = h_3\mathbf{I} + h_4\mathbf{J}$, $m = \left[\dfrac{1}{\tau_r}\left(h_1 + \dfrac{R_s}{\sigma L_s} + \dfrac{h_3}{c}\right) + \omega_r\left(h_2 + \dfrac{h_4}{c}\right)\right]$,

$n = \left[\dfrac{1}{\tau_r}\left(h_2 + \dfrac{h_4}{c}\right) - \omega_r\left(h_1 + \dfrac{R_s}{\sigma L_s} + \dfrac{h_3}{c}\right)\right]$,

$x = \left(h_1 + \dfrac{R_s}{\sigma L_s} + \dfrac{h_3}{c}\right)$, and $y = \left(h_2 - \omega_r\right)$.

Using the stator current estimation error, $\mathbf{e_i}$ and the estimated rotor flux, $\hat{\boldsymbol{\lambda}}_r$, the electrical rotor speed can be estimated as (8) with the widely used proportional-integral (PI) compensator due to its practical simplicity.

$$\hat{\omega}_r = K_P(\mathbf{J}\hat{\boldsymbol{\lambda}}_r)^T\mathbf{e_i} + K_I\int(\mathbf{J}\hat{\boldsymbol{\lambda}}_r)^T\mathbf{e_i}dt \tag{8}$$

III. Gain Design of an Adaptive Full-Order Observer

Fig. 2(a) shows a block diagram of the speed estimation in the stationary reference frame, and Fig. 2(b) depicts the transformed version of Fig. 2(a) in the rotor flux reference frame. The transfer function from the speed estimation error to the *q*-axis stator current estimation error in the rotor flux reference frame, $G'_{22}(s)$, can be derived as (9). Detailed explanations of Fig. 2 and (9) are described in [7].

$$G'_{22}(s) \cong \frac{1}{c}\frac{s^3 + xs^2 + (\omega_e^2 + m)s + \omega_e^2 x + \omega_e n}{\left(s^2 + xs - \omega_e^2 - \omega_e y + m\right)^2 + \left((2\omega_e + y)s + \omega_e x + n\right)^2} \tag{9}$$

where ω_e means the synchronous speed of an induction motor. Using (9), the transfer function from the actual rotor speed to the estimated speed $\left(\hat{\omega}_r / \omega_r\right)$ is described as (10).

$$\frac{\hat{\omega}_r}{\omega_r} = \frac{|\lambda_r|^2 G'_{22}(s)(K_P + K_I/s)}{1 + |\lambda_r|^2 G'_{22}(s)(K_P + K_I/s)} \tag{10}$$

As shown in (9) and (10), the performances of an adaptive full-order observer are determined by the observer gain matrix, **H**, and the speed estimation gains. Thus, the observer gain design strategy plays a major role in the observer's performance.

A. Conventional Method

One of the conventional gain design methods of an adaptive full-order observer is that the poles of the adaptive full-order observer are placed proportional to those of the induction machines [6]. In this case, the characteristic equation of the adaptive full-order observer and the elements of the observer gain matrix are given as (11) and (12), respectively, when the poles of the adaptive full-order observer are ' k ' times that of the induction machine.

$$\begin{aligned}&s^2 - \left\{\left(a_{r11} + a_{r22} - h_1\right) + j\left(\hat{a}_{i22} - h_2\right)\right\}s \\ &-\left(a_{r12} + j\hat{a}_{i12}\right)\left\{ca_{r11} - ch_1 + a_{r21} - h_3 + j\left(-ch_2 - h_4\right)\right\} = 0\end{aligned} \tag{11}$$

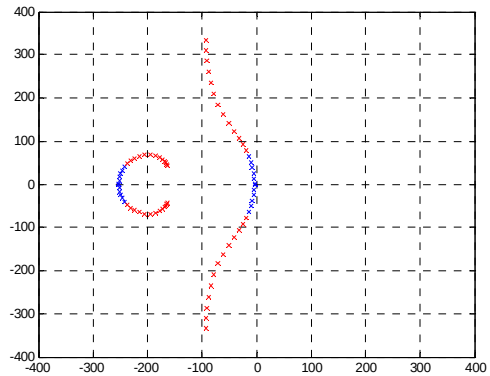

Fig. 3. Example of pole movements using the conventional method (3.7-kW, 4-pole, 200-V induction machine).

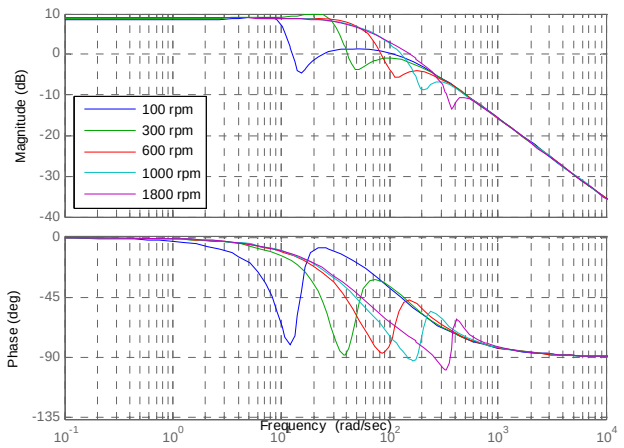

Fig. 4. Bode plot of $G_{22}^{'}(s)$ of the conventional method (3.7-kW, 4-pole, 200-V induction machine).

$$h_1 = (1-k)(a_{r11}+a_{r22}), \quad h_2 = (1-k)\hat{a}_{i22},$$
$$h_3 = (1-k^2)(ca_{r11}+a_{r21})+c(k-1)(a_{r11}+a_{r22}), \quad (12)$$
$$h_4 = c(k-1)\hat{a}_{i22}.$$

Fig. 3 shows an example of the pole location of an adaptive full-order observer when the proportional gain, k, is set to '1'. A 3.7-kW, 4-pole, 200-V induction machine is used in this example. Under low-speed operation (10~500 r/min, blue marks), two dominant poles are located near the origin and two other poles are positioned near −250 rad/s. Because the natural frequency of the dominant poles increases with speed, the estimation performance is maintained at low speeds. Nevertheless, when the operating speed is very low, the natural frequency is almost zero. As a result, the estimation performance may be insufficient for stable operation when there is a sudden step load.

At higher speeds (600~1800 r/min, red marks, Fig. 3), the dominant poles move toward the imaginary axis, and the other poles move toward the real axis. As the speed increases, the dominant poles switch to the other poles, and the natural frequency of the observer becomes smaller than the operating frequency. This degrades the estimation performance of the observer as the speed increases. In addition, unstable operation may occur at high speeds.

In industrial fields, the proportional gain, k, has a set value of 1.1~1.5 under low-speed operation. At high speeds, the gain is set to 2.0~4.0. These values were selected based on empirical results.

Fig. 4 shows a Bode plot of $G_{22}^{'}(s)$ using the conventional method [6], which is based on rotor speed. The phase shift reaches up to nearly −90 degrees and increases slightly as the speed increases. Because $G_{22}^{'}(s)$ is included in the speed estimation loop, as shown in Fig. 2(b), the speed estimation performance of the adaptive full-order observer with the conventional feedback gain is expected to be unstable.

B. Stability Conditions

As shown in Fig. 2(b), $G_{22}^{'}(s)$ is included in the speed estimation loop. $G_{22}^{'}(s)$ refers to the transfer function from the speed estimation error to the q-axis stator current estimation error in the rotor flux reference frame. To achieve stable speed estimation, the stability of the speed estimation loop including $G_{22}^{'}(s)$ should be considered.

Specifically, the stable pole and stable zero conditions of $G_{22}^{'}(s)$ can be used to determine the stability conditions of the speed estimation. The stable pole conditions of $G_{22}^{'}(s)$ are generally valid. Even without the feedback of the observer ($H_1 = 0$, $H_2 = 0$), the observer poles are stable. With an appropriate observer gain, the observer poles lie strictly in the left-half plane.

Considering the high adaptation PI gain usually used in speed estimation to achieve fast tracking of a speed change, the speed estimation loop can be considered as a high gain feedback system. In a high gain feedback system, the closed-loop poles move toward the open-loop zeros. As a result, stable zeros of $G_{22}^{'}(s)$ are required. Specific conditions are necessary to achieve stable zero conditions. Among these conditions, the following condition is the most restrictive for stability [8]:

$$\omega_e(\omega_e - \omega_c) > 0 \quad (13)$$

$$\omega_c = -\frac{n}{x} = -\frac{\left[\frac{1}{\tau_r}\left(h_2+\frac{h_4}{c}\right)-\omega_r\left(h_1+\frac{R_s}{\sigma L_s}+\frac{h_3}{c}\right)\right]}{\left(h_1+\frac{R_s}{\sigma L_s}+\frac{R_r}{\sigma L_r}\right)} \quad (14)$$

where ω_e and ω_c refer to the operating frequency and the critical frequency, respectively. The stable operation area of the observer is determined by the observer feedback gain as (13) and (14). If the critical frequency is not zero, then an unstable region exists. When the conventional gain design

method [6] is adopted, ω_c is non-zero. Therefore, an unstable region exists.

For the stable operation area to expand over the entire operating range, the critical frequency must be zero. As a result, stable operation can be achieved over the entire range, with the exception of zero operating frequency. Detailed analyses of the above descriptions are described in [8]. Along with the above analysis, several gain design strategies of the observer have been presented in the literature [7], [9], [16]-[20].

C. Proposed Pole Placement Method

As described above, the stability and estimation performance of the observer depend on the observer's feedback gains. The poles and zeros of the observer are also determined by the gains. Therefore, the observer gains can be designed by placing the poles at desired positions. Based on this insight, in order to investigate where the poles should be located, the observer poles are placed arbitrarily. The characteristic equation of the observer can be described by (11), and the arbitrary pole positions are given by (15):

$$pole_1 = -x_1 - jy_1, \quad pole_2 = -x_2 + jy_2 . \tag{15}$$

where x_1, x_2, y_1, and y_2 are positive. Equation (16) describes the characteristic equation, which has the pole positions given in (15). Comparing (11) and (16), the observer gains can be determined as given in (17). Because the observer has conjugate roots in reality, the observer has four poles, as given by (18):

$$\begin{aligned} & s^2 + \left[(x_1 + x_2) + j(y_1 - y_2)\right]s + \\ & \quad \left[(x_1 x_2 + y_1 y_2) + j(x_2 y_1 - x_1 y_2)\right] = 0 \\ \Leftrightarrow \quad & s^2 + \left[A + jB\right]s + \left[C + jD\right] = 0. \end{aligned} \tag{16}$$

$$\begin{aligned} & h_1 = a_{r11} + a_{r22} + A, \quad h_2 = \hat{\omega}_r + B, \\ & h_3 = a_{r21} - c a_{r22} - cA - \frac{c\tau_r\left[C + \hat{\omega}_r \tau_r D\right]}{(\hat{\omega}_r \tau_r)^2 + 1}, \\ & h_4 = -c\hat{\omega}_r - cB - \frac{c\tau_r\left[\hat{\omega}_r \tau_r C - D\right]}{(\hat{\omega}_r \tau_r)^2 + 1}. \end{aligned} \tag{17}$$

$$pole_{1,3} = -x_1 \pm jy_1, \quad pole_{2,4} = -x_2 \pm jy_2 . \tag{18}$$

Using the observer gains of (16), the critical frequency can be simplified as given in (19). When the poles are placed strictly in the left-half plane, A is always positive and D depends on the pole positions. For the critical frequency to be zero, D should be zero. This condition is represented by (20), and the corresponding pole positions are shown in the complex domain of Fig. 5. The angles between the two poles and the real axis are the same. Therefore, by placing the observer poles as shown in Fig. 5, the critical frequency is zero and the unstable operating region is minimized.

$$\omega_c = -\frac{D}{A} \tag{19}$$

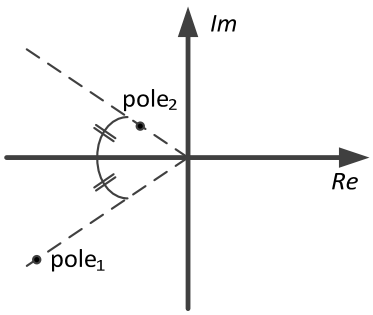

Fig. 5. Pole position diagram when the critical frequency is zero.

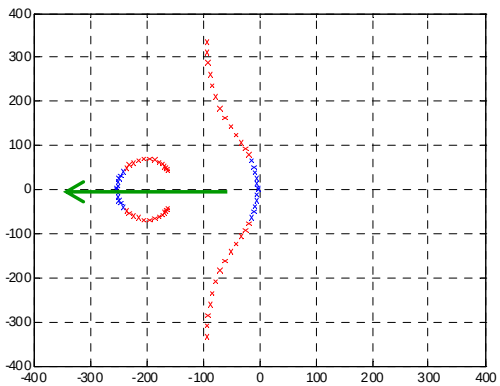

Fig. 6. Pole placement of the proposed method (green, 3.7-kW, 4-pole, 200-V induction machine).

$$\frac{y_1}{x_1} = \frac{y_2}{x_2} \qquad (x_1, x_2, y_1, y_2 > 0) \tag{20}$$

Moreover, when the poles of an adaptive full-order observer have a fixed value, the estimation performance of the observer can become degraded at high speeds [21]. Therefore, the poles of the observer should be moved according to the rotor speed in order for the observer to have enough estimation performance.

Considering the condition in Fig. 5, the characteristic equation is selected as (21), and the corresponding gains of the observer are described by (22):

$$s^2 + 2\varsigma\omega_n s + \omega_n{}^2 = 0 . \tag{21}$$

$$\begin{aligned} & h_1 = a_{r11} + a_{r22} + 2\varsigma\omega_n, \quad h_2 = \hat{\omega}_r, \\ & h_3 = a_{r21} - c a_{r22} - 2c\varsigma\omega_n - c\omega_n^2 \tau_r \frac{1}{(\hat{\omega}_r \tau_r)^2 + 1}, \\ & h_4 = -c\hat{\omega}_r - c\omega_n^2 \tau_r \frac{\hat{\omega}_r \tau_r}{(\hat{\omega}_r \tau_r)^2 + 1}. \end{aligned} \tag{22}$$

For simplicity, the damping coefficient can be selected as one. In this case, the observer has a quadruple pole which lies in the real axis. In addition, to improve the estimation performance as described above, the poles of the adaptive full-order observer should move in the direction of the negative real axis. Thus, the natural frequency, ω_n, is set as the absolute value of the electric rotor speed. In practice, the natural frequency of the proposed strategy has a minimum

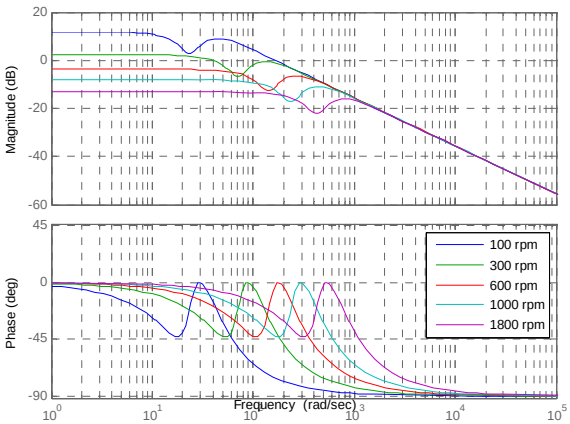

Fig. 7. Bode plot of $G_{22}^{'}(s)$ of the proposed method (3.7-kW, 4-pole, 200-V induction machine).

TABLE I
NOMINAL PARAMETERS OF THE TESTED INDUCTION MACHINE

Parameters	Values [unit]
Rated power	3.7 [kW]
Rated speed	1745 [r/min]
Rated frequency	60 [Hz]
Number of poles	4
Rated voltage	220 [V]
Rated current	14.1 [A]
Stator resistance	0.384 [Ω]
Rotor resistance	0.336 [Ω]
Magnetizing inductance	66.547 [mH]
Transient inductance	5.9 [mH]

value, ω_{n_MIN}, to procure the operation of the adaptive observer at low speeds, including zero frequency. The proposed pole placement is demonstrated in Fig. 6 and Fig. 3.

Fig. 7 shows a frequency analysis $G_{22}^{'}(s)$ of the proposed strategy, which was obtained using the rotor speed. The phase shift of $G_{22}^{'}(s)$ is greatly reduced, up to −45 degrees. The phase shift of the conventional method is twice that of the proposed method. Based on the difference in the phase shift, it can be expected that the stability of the speed estimation will be enhanced.

The critical difference between the conventional method and the proposed method is the pole placement, as shown in Fig. 6. In the conventional method, the poles of the observer are placed proportional to those of the induction machine. The ratio between the observer poles and the machine poles is adjusted by the gain, k. Therefore, the observer poles of the conventional method are placed at k times the machine poles. According to the operating speed and the gain, k, the poles are determined at specific positions in the left half plane. The estimation performance might be insufficient in some cases. For example, when the operating speed is 1800 r/min, the dominant pole of the IM is about -160 ± j10. When k is equal to 1, the observer pole is the same as that of the IM. As a result, the estimation performance is degraded.

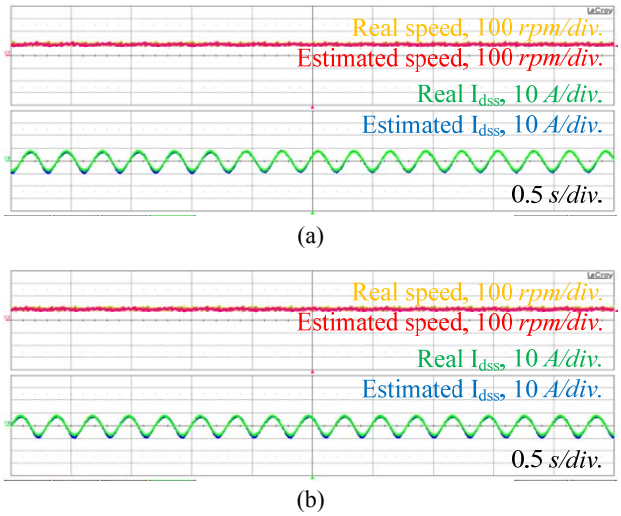

Fig. 8. Comparison of the stator current estimation performance under low-speed operation (100 r/min): (a) conventional method and (b) the proposed method.

On the other hand, the observer poles of the proposed method are placed according to the natural frequency, ω_n and the damping coefficient. By determining the damping coefficient as one, the poles can be place in the real axis. In addition, by setting the natural frequency as the absolute value of the electrical rotor speed, the observer pole can move toward the negative real axis. Therefore, appropriate estimation performance can be maintained under overall operating conditions.

The main advantages of the proposed gain design strategy are as follows.

1. Minimization of the unstable operation region.
2. The observer has minimum pole positions, ω_{n_MIN}, even at zero operating frequency. As a result, the estimation capability is maintained.
3. The estimation performance is satisfactory over the entire operating range, even under overloaded conditions. This will be shown in Section IV.

IV. EXPERIMENTAL RESULTS

Experiments were conducted to show the effectiveness of the proposed feedback gain design. The tested machine was a 3.7-kW induction machine. A 5-kW surface-mounted permanent magnet synchronous machine was used as a load. Table I shows the nominal parameters of the tested machine. The induction motor was driven by the proposed sensorless algorithm in the speed control mode, and the load machine was driven in the torque control mode with an encoder. The pulse width modulation (PWM) was based on space vector PWM. The sampling and switching period were set to 100 μs and 200 μs, respectively. The dead-time was 3 μs. The bandwidths of the speed and current controller were set to 5 Hz and 250 Hz, respectively.

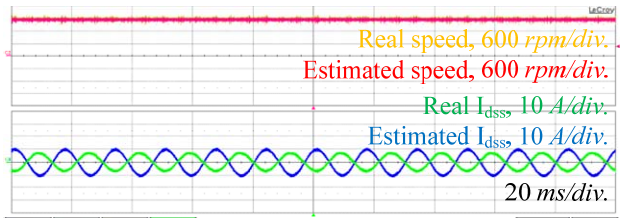

(a)

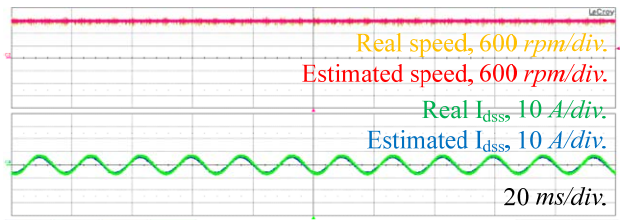

(b)

Fig. 9. Comparison of the stator current estimation performance under high-speed operation (1800 r/min): (a) conventional method and (b) the proposed method.

Fig. 8 shows a comparison of the experimental results for stator current estimation performance between the cases of a conventional observer [6] and the proposed observer, at a low speed of 100 r/min. The observer gains for the conventional and the proposed method were set as (12) and (22), respectively. In the conventional method, k was set as 1.3. In the proposed method, ω_n is set as the absolute value of the electric rotor speed. For simplicity, the damping coefficient is selected as one. The proportional and integral gains of the speed adaptation were selected as 5 and 6000, respectively. These values were selected based on empirical results. The real and estimated speeds are shown together in the upper grid, and the real and estimated *d*-axis stator current in the stationary reference frame are shown in the lower grid (Fig. 8). In both cases, the speed and the *d*-axis stator current were well estimated. Sufficient estimation performance was demonstrated by the observers at the given frequency.

Fig. 9 shows similar waveforms at a high speed of 1800 r/min. Both cases demonstrated good speed estimation. However, the current estimation performance of the conventional method was poor (Fig. 9(a)), and the phase of the estimated current was explicitly shifted. The reason for the shift can be described as follows. When the operating speed is 1800 r/min, the frequency of the current is 60 Hz (377 rad/s). However, as shown in Fig 3, the dominant poles of the observer of the conventional method are located at about -160 ± j40, whose natural frequency is 165 rad/s which is smaller than 377 rad/s. It can be deduced that the error of the current estimation came from the fact that the dominant pole of the conventional observer had an insufficient value to estimate the state variables (*e.g.*, the stator current and the rotor flux).

On the other hand, the results based on the proposed method, shown in Fig. 9(b), show better estimation performance for the stator current than that of the conventional approach, even under high-speed operation. This is because the observer pole positions of the proposed method were adjusted toward the negative real axis according to the operating speed of the induction machine, which resulted in better estimation. Based on the estimation performances, the induction motor was driven by a direct vector control technique in the step load tests described below.

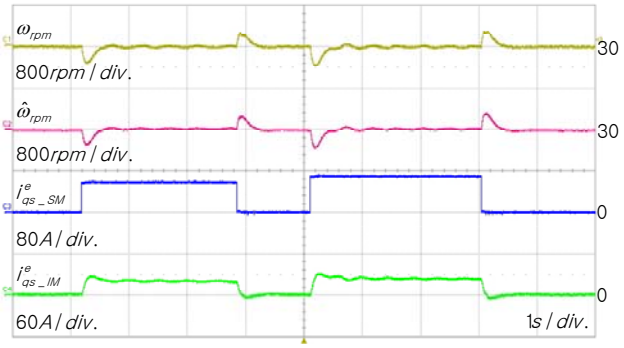

Fig. 10. Experimental results at 1 Hz (30 r/min) in motoring mode; 125% and 150% step load applied.

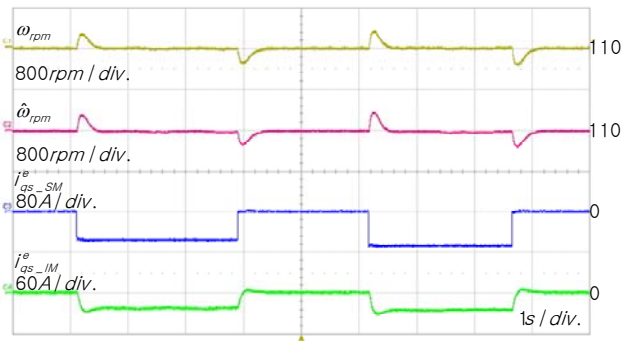

Fig. 11. Experimental results at 110 r/min in regenerating mode; 125% and 150% step load applied.

Due to the enhanced estimation performance, the overall operations of the sensorless control showed stable performances, even for overloads of 150 %. Fig. 10 shows the performance of the speed sensorless control, with proposed feedback gains under 1-Hz (30 r/min) motoring operation. Step loads of 125 % and 150 % were applied. From top to bottom, the real speed, the estimated speed, and the *q*-axis current of the load machine, along with those of the tested induction machine are demonstrated together. While there were small ripples in the waveforms, the operation was stable even under a 150% step load.

Fig. 11 shows the performance of the induction machine under regeneration operation. Similarly, 125% and 150% step loads were applied. The operating speed was 110 r/min, which is twice the rated slip frequency of the test machine. As shown in the figures, the induction machine performed well, even under overloaded conditions. The sensorless operation was also very responsive during the regenerating mode.

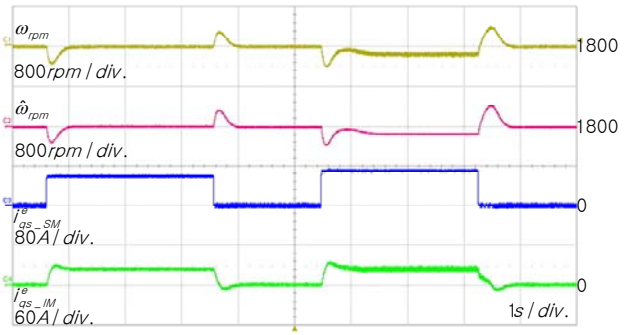

Fig. 12. Experimental results at 1800 r/min in motoring mode; 125% and 150% step load applied.

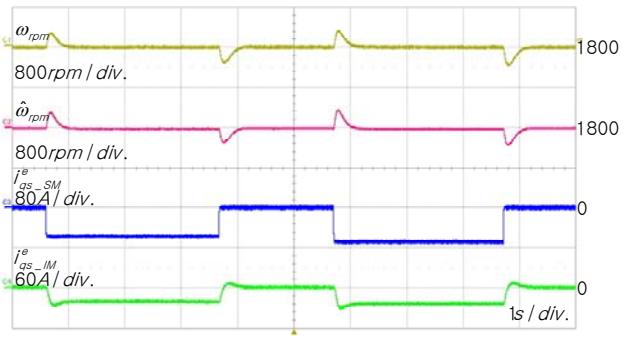

Fig. 13. Experimental results at 1800 r/min in regenerating mode; 125% and 150% step load applied.

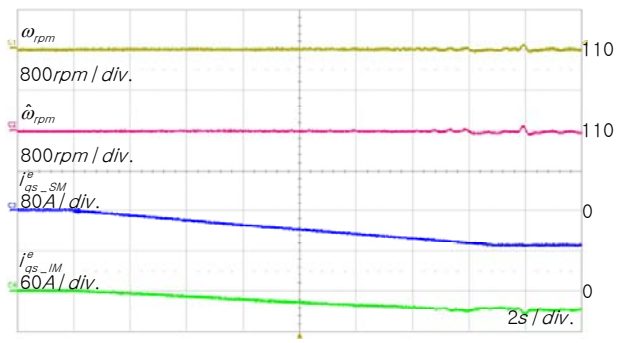

Fig. 14. Experimental results at 110 r/min in regenerating mode; 150% ramp load applied.

Fig. 12 and Fig. 13 show the high-speed operation performances at 1800 r/min under the motoring and regenerating mode, respectively. Similarly, 125 % and 150 % step loads were applied. Under the motoring mode with a 150 % load, the rotor speed was less than 1800 r/min due to the lack of the output voltage of the inverter. In the experiment, as shown in Fig. 12, a flux weakening control was not adopted. Using a proper flux weakening algorithm, 1800 r/min operation would be possible. As shown in these figures, the speed sensorless operation with the proposed method was also stable in high-speed operations, even under insufficient output voltage conditions.

Fig. 14 shows the experimental results under the slow load change condition. Ramp loads were applied, and the loads changed from 0 % to 150 % for 15 s. This was regeneration operation and the operating speed was 110 r/min. As the load increased, the synchronous frequency decreased. When 150 % loads were applied, the frequency was 0.9 Hz. Even under the overloaded condition of 150 %, it showed stable operations.

Based on these experimental results, it can be concluded that with the proposed feedback gain, the speed sensorless drives of induction machines work well over the entire operating region.

V. CONCLUSIONS

This paper presents a generalized gain design strategy for the adaptive full-order observers of induction machines in speed sensorless control. The unstable operating region was minimized. In addition, this paper proposes that the poles of the adaptive full-order observer should move in the direction of the negative real-axis, according to the rotor speed. Under these guidelines the analysis showed that the proposed design significantly improved the performance of speed sensorless drives. The effectiveness of the proposed strategy was verified by experimental results.

ACKNOWLEDGMENT

This work was supported by the Human Resources Program in Energy Technology (No. 20134030200310) of the KETEP, granted financial resource from the MOTIE (Ministry of Trade, Industry & Energy) of Korea and the Basic Science Research Program (NRF-2014R1A1A1005138) through the NRF of Korea funded by the MSIP(Ministry of Science, ICT & Future Planning) of Korea.

REFERENCES

[1] B.Metidji, N. Taib, L. Baghli, T. Rekioua, and S. Bacha, "Low-cost direct torque control algorithm for induction motor without ac phase current sensors," *IEEE Trans. Power Electron.*, Vol. 27, No. 9, pp. 4132-4139, Sep. 2012.

[2] Y. Liu, J. Zhao, R. Wang, and C. Huang, "Performance improvement of induction motor current controllers in field-weakening region for electric vehicles," *IEEE Trans. Power Electron.*, Vol. 28, No. 5, pp. 2468-2482, May 2013.

[3] P. Vas, *Sensorless Vector and Direct Torque Control*, New York, NY, USA: Oxford Univ. Press, 1998, pp. 122–124.

[4] T. Ohtani, N. Takada, and K. Tanaka, "Vector Control of Induction Motor without Shaft Encoder," *IEEE Trans. Ind. Appl.*, Vol. 28, No. 1, pp. 157-164, Jan./Feb. 1992.

[5] K. Ohyama, G. M. Asher, and M. Summer, "Comparative analysis of experimental performance and stability of sensorless induction motor drives," *IEEE Trans. Ind. Electron.*, Vol. 53, No. 1, pp. 178-186, Feb. 2006.

[6] H. Kubota, K. Matsuse, and T. Nakano, "DSP-based control of the induction machine," *IEEE Trans. Ind. Appl.*, Vol. 29, No .2, pp. 344-348, Mar/Apr, 1993.

[7] S. Sangwongwanich and S. Suwankawin, "Design strategy of an adaptive full-order observer for speed-sensorless induction-motor drives-tracking performance and stabilization," *IEEE Trans. Ind. Electron.*, Vol. 53, No. 1, pp. 96-119, Feb. 2006.
[8] S. Sangwongwanich and S. Suwankawin, "A speed-sensorless IM drive with modified decoupling control," *IEEE Trans. Ind. Electron.*, Vol. 49, No. 2, pp. 444-455, April 2002.
[9] S. Sangwongwanich, S. Suwankawin, and S. Koonlaboon, "A unified speed estimation design framework for sensorless ac motor drives based on positive-real property," in *Proc. PCC-Nagoya 2007*, pp. 1111-1118, 2007.
[10] L. Harnefors and M. Hinkkanen, "Complete stability of reduced-order and full-order observers for sensorless IM drives," *IEEE Trans. Ind. Electron.*, Vol. 55, No. 3, pp. 1319-1329, Mar. 2008.
[11] P. L. Jansen and R. D. Lorenz, "A physically insightful approach to the design and accuracy assessment of fulx observers for field oriented induction motors," *IEEE Trans. Ind. Appl.*, Vol. 30, not. 1, pp. 1052-1060, Jul./Aug. 2003.
[12] J. Holtz and J. Quan, "Drift- and parameter-compensated flux estimator for persistent zero-stator-frequency operation of sensorless-controlled induction motors," *IEEE Trans. Ind. Appl.*, Vol. 39, No. 4, pp. 1052-1060, Jul./Aug. 2003.
[13] M. Tsuji, S. Chen, K. Izumi, and E. Yamada, "A sensorless vector control system for induction motors using q-axis flux with stator resistance identification," *IEEE Trans. Ind. Electron.*, Vol. 48, No. 1, pp. 185-194, Feb. 2001.
[14] M. Rashed and A. F. Stronach, "A stable back-EMF MRAS-based sensorless low-speed induction motor drive insensitive to stator resistance variation," *IEE Proc. Electr. Power Appl.*, Vol. 151, No. 6, pp. 685-693, Nov. 2004.
[15] C. Lascu, I. Boldea, and F. Blaabjerg, "Very-low-speed variable-structure control of sensorless induction machine drives without signal injection," *IEEE Trans. Ind. Appl.*, Vol. 41, No. 2, pp. 591-598, Mar./Apr. 2005.
[16] M. Saejia and S. Sangwongwanich, "Averaging analysis approach for stability analysis of speed-sensorless induction motor drives with stator resistance estimation," *IEEE Trans. Ind. Electron.*, Vol. 53, No. 1, pp. 162-177, Feb. 2006.
[17] M. Hinkkanen, L. Harnefors, and J. Luomi, "Reduced-order flux observers with stator-resistance adaptation for speed-sensorless induction motor drives," *IEEE Trans. Power Electron.*, Vol. 25, No. 5, pp. 1173-1183, May 2010.
[18] M. S. Zaky, "Stability analysis of speed and stator resistance estimators for sensorless induction motor drives," *IEEE Trans. Ind. Electron.*, Vol. 59, No. 2, pp. 858-870, Feb. 2012.
[19] Z. Qu, M. Hinkkanen, and L. Harnefors, "Gain scheduling of a full-order observer for sensorless induction motor drives," *IEEE Trans. Ind. Appl.*, Vol. 50, No. 6, pp. 3834-3845, Nov./Dec. 2014.
[20] B. Chen, W. Yao, K. Wang, K. Lee and Z. Lu, "comparative analysis of feedback gains for adaptive full-order observers in sensorless induction motor drives," *in Conf. Rec. IEEE-ECCE 2013*, pp. 3481-3487, Sep, 2013.
[21] K. Kim and I. Kim, "Design of discrete flux observer by the power series approximation," *Journal of Power Electronics*, Vol.11, No. 3, pp. 304-310, May 2011.

Anno Yoo received his B.S., M.S., and Ph.D. degrees in Electrical Engineering from Seoul National University, Seoul, Korea, in 2004, 2006, and 2010, respectively. From 2010 to 2015, he was a Senior Research Engineer with LSIS Co., Ltd., Anyang, Korea. From 2015 to 2016, he was a Senior Research Engineer with Mando Corporation, Seongnam, Korea. Since 2016, he has been a Senior Motor Controls Engineer with General Motors, Pontiac, Michigan, United State. His current research interests include high performance electric machine drives, electric machine modeling, and power conversion system for electric/hybrid vehicles. He is holder of 6 registered patents in the United State and was a recipient of the 2015 Best Paper Award of the *Journal of Power Electronics* (2nd Prize).

Sang-Heon Han was born in Korea, in 1991. He received his B.S. degree in Electrical Engineering from Myongji University, Yongin, Korea, in 2009; where he has been working towards his M.S. degree, since 2015. His current research interests include the power electronic control of electric machines, sensorless drives, and power conversion circuits.

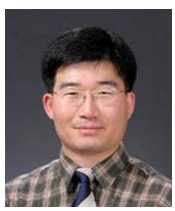

Young Ik Son received his B.S., M.S., and Ph.D. degrees from Seoul National University, Seoul, Korea, in 1995, 1997 and 2002, respectively. From 2007 to 2008, he was a Visiting Scholar at Cornell University, Ithaca, New York. Since 2003, he has been with the Department of Electrical Engineering at Myongji University, Yongin, Korea, where he is presently working as a Professor. His current research interests include robust controller design and its application to industrial electronics. He has served as an Editorial Board Member of the *International Journal of Control, Automation, and Systems*.

Young-Doo Yoon was born in Korea. He received his B.S., M.S., and Ph.D. degrees in Electrical Engineering from Seoul National University, Seoul, Korea, in 2002, 2005, and 2010, respectively. From 2010 to 2013, he was with Samsung Electronics Company, Korea, as a Senior Engineer. Since 2013, he has been an Assistant Professor in the Department of Electrical Engineering, Myongji University, Yongin, Korea. His current research interests include the power-electronic control of electric machines, high power converters, and electric home appliances.

Chanook Hong received his B.S. and M.S. degrees from Seoul National University, Seoul, Korea, in 1991 and 1993, respectively. Since 1993, he has been with LS Industrial Systems., Ltd., Anyang, Korea, where he is presently working as the Team Manager. His current research interests include high performance motor control and power conversion.